Numerical fluid flow modelling and its seismic response in time-lapse

Vanja Milicevic and Robert J. Ferguson
CREWES Project, University of Calgary

Summary

A time-lapse reservoir characterization study is performed on a model of a producing reservoir. This model reservoir has two injection wells and one producer. Pressure and saturation models are obtained from numerical simulation of reservoir properties and fluid flow for a number of calendar days. Integration of saturation models and Gassmann's relations delivers compressional wave velocity models for each calendar day, and finite-difference algorithms are used to generate synthetic data for comparison; specifically, we compare 2D acoustic and 3C-3D elastic forward modelling. Examples show subtle similarities and differences between the models and both prove to be valuable tools in reservoir characterization.

Introduction

Development of a reservoir depends on the alliance of geologists, geophysicists and engineers. These scientists localize the reservoir and when infrastructure is set, production begins (Hubbard, personal communication). Eventually the primary production recovery becomes uneconomical due to reservoir depletion (Cosse, 1993). At this time artificial recovery methods, whose success depends on reservoir familiarity, are employed (Cosse, 1993). This is not difficult for reservoirs with long production history, however, it is a challenging task in reservoirs with short to no production history (Vracar, 2007). Now, numerical modelling of injection flow allows visualization and analysis of reservoir properties (Aarnes, 2007).

As Stoffa (2008) experimentally shows fluid injection causes seismic response changes. Gassmann's relations tie fluid flow to density saturation, P-wave and S-wave velocities (Mavko, 2009). Chakraborty (2007) shows fluid flow changes, using Gassmann's relations, trigger changes in time-lapse seismic responses. In this paper, we map fluid flow to seismic response focusing on compressional (P) wave velocity models. We generate and evaluate events on both acoustic and elastic time-lapse models.

The designed time-lapse study follows three stages: 1) flow modelling, 2) rock physics, and 3) seismic modelling. Stage I employs flow modelling using reservoir simulator to calculate pressure and saturation through reservoir properties. Stage II employs rock physics to calculate density and compressional (P) wave velocity. Stage III employs P-wave velocity to generate seismic models in 2D and 3C-3D. 2D models are generated invoking exploding reflectors algorithm in acoustic medium. 3C-3D models are generated using a single shot gatherer in elastic medium. Both methods prove to be valuable.

Theory

Numerical Fluid Flow
Assume a homogeneous and isotropic reservoir with constant porosity and incompressibility for simulation. The elliptic equation for phase pressure conserved in time-lapse is as follows (Aarnes et al., 2007):

$$\nabla \cdot v_{f,p} = \frac{q_p}{\rho_p} \ , \tag{1}$$

where $v_{f,p}$, q and ρ are flow velocity, inflow/outflow and density of the phase, respectively. Equation (1) describes pressure gradient constant in each grid box over time and its variance

from grid box to grid box. Consider the following equation (Aarnes, 2007):

$$\phi \frac{\partial s}{\partial t} + \nabla f(s) v_{f,p} = \frac{q_p}{\rho_p} ,$$

(2)

where ϕ, s and t are porosity, saturation and time, respectively. Equation (2) estimates saturation from the reservoir conditions and water flow in each grid box. The numerical modelling of fundamental reservoir system is done employing equations (1) and (2).

Rock Physics
Gassmann's equations produce velocity models from saturation models. Mavko (2009) states:

$$K_{sat} = K_d + \frac{\left(1 - \frac{K_d}{K_0}\right)^2}{\frac{\phi}{K_f} + \frac{(1-\phi)}{K_0} - \frac{K_d}{K_0^2}} \quad \text{and} \quad \mu_{sat} = \mu_d$$

(3)

where K_{sat}, K_f, K_d, and K_0 are the effective bulk modulus of saturated rock, the effective bulk modulus of pore fluid, the frame bulk modulus of dry rock and the bulk modulus of mineral material making up the rock, respectively. The saturated shear modulus and the dry shear modulus, μ_{sat} and μ_d, respectively, are independent of saturation (Mavko, 2009). Now invoke density saturation, ρ_{sat}:

$$\rho_{sat} = (1 - \phi)\rho_0 + \phi\rho_f ,$$

(4)

where ρ_0 and ρ_f are matrix density and fluid density. Combination of equations (3) and (4) yields P-wave velocity, α, (Mavko, 2009):

$$v_p = \frac{\sqrt{K_{sat} + \frac{4}{3}\mu_{sat}}}{\rho_{sat}} .$$

(5)

Seismic Models
Using equation (5), we are able to generate seismic density plots in acoustic and elastic medium employing finite difference algorithm. The reservoir top and bottom reflections are expected to be stationary on all plots in time-lapse. The waterfronts are anticipated to map sooner as time progresses. We expect no variation, when laterally correlating density above and below waterfronts in time-lapse. Density above waterfronts alone maps no change in time-lapse.

Examples
Data Description
Designed work flow is applied to the 10th SPE Comparative Solution Project (Christie, 2001) for verification. The reservoir is initially 100% oil saturated. A single producer is located in the center of the reservoir, while two injectors are situated on the left and right side of the producer at equal distances. The study models two-phase flow, oil production simulation through water injection in 28 days. The study's duration is short due to the stable reservoir conditions and low mobility ratio. The phases are immiscible and incompressible. Water and oil saturations are irreducible (Aarnes, 2007). The reservoir boundaries are impermeable. A public domain numerical simulator, provided by SINTEF ICT, is used to model such fluid flow (Aarnes, 2007).

Observation of both water saturation and pressure models prove these two parameters to decrease from injectors to producer. Further employing Gassmann's relations to calculate density saturation and P-wave velocity, we observe a decrease from injectors to producer.

Now, the above P-wave velocity profiles are used to create 2D exploding reflector seismic gathers employing function *afd_explode* from the MATLAB CREWES Project toolbox. Figure 1

shows the exploding reflector gather after day 1, 14 and 28. Observe reservoir top and bottom, denoted by red and green arrows respectively, to stay stationary until day 28. Both waterfronts, denoted by yellow arrows, create bow-tie effect. They are non-stationary and propagate upward in time. Observe a water breakthrough at the producer. The amplitude dims as water saturation increases. Note reservoir top, bottom and waterfronts appear in opposite polarity reflection coefficients.

The 3C-3D seismic models in elastic medium are generated using Tiger, commercial software designed by SINTEF ICT. Observe each component individually. Figures 2(a), (b) and (c), x-component velocity models, show S-waves. Reservoir boundaries, as white arrow, appear as slanted linear events. A weak projection of P-waves from z-component is seen at about 2.0s and at about 2.2s. Two projections are inferred to be reservoir top and waterfronts, denoted by red and yellow arrows, respectively. Observed in time-lapse waterfronts progress upwards. Figures 4(a), (b) and (c), y-component velocity models, capture converted waves, that is P-waves reflected as S-waves. Both reservoir boundaries show as slanted linear events noted by white arrow. We note reservoir top and bottom, pointed to by red and green arrows, at about 1.6s and 2.1s, respectively. Also note two waterfronts, pointed to by yellow arrows, progressing upwards with time. Numerical artifacts are denoted by magenta arrow. Rayleigh waves are pointed to by black arrow. Figures 5(a), (b) and (c) are z-component velocity models. These models are directly comparable to the acoustic models. The reservoir top and bottom are denoted by red and green arrows, respectively. Reservoir bottom is seen as a set of high-low-high amplitudes. Reservoir top shows as low-high-low set of amplitudes, later smeared by a set of high-low-high amplitudes after 28 days. The waterfronts, denoted by yellow arrows, create a bow-tie effect progressing upward in time. The pattern of reversed polarity between reservoir top, bottom and waterfronts still applies. Note S-wave projection from x-component, marked by the turquoise arrow, at about 1.18s, stationary in time-lapse. Numerical artifacts are denoted by magenta arrow. Rayleigh waves are pointed to by black arrow. Examples prove work flow feasible.

Conclusions

A time-lapse study takes place on a reservoir employing one producing and two injecting wells. The study follows three stages: numerical simulation, Gassmann's relations and finite-difference algorithm. The numerical simulation of fluid flow produces saturation and pressure models. Then, the saturation models deliver P-wave velocity models as a result of Gassmann's relations. Further, P-velocity models, through finite-difference algorithms, generate 2D acoustic and 3C-3D elastic seismic models. The theoretical concepts are verified through numerical examples. There are subtle similarities and differences between acoustic and elastic models. Study proves both, acoustic and elastic models, to be assets to reservoir characterization.

Acknowledgements

References

Aarnes, J. E., Gimse, T., and Lie, K. A., 2007, An introduction to the numerics of flow in porous media using matlab, *in* Hasle, G., Lie, K., and Quak, E., Eds., Numerical Simulation, and Optimization: Applied Mathematics at SINTEF, Springer, 265–306.

Charkraborty, S., 2007, An integrated geologic model of valhall oil field for numerical simulation of fluid flow and seismic response: M.Sc. thesis, University of Texas at Austin.

Christie, M. A., and Blunt, M. J., 2001, Tenth SPE comparative solution project: A comparison of upscaling techniques: SPE Reservoir Engineering and Evaluation, Society of Petroleum Engineers, **4**, 308–317.

Cosse, R., 1993, Basics of Reservoir Engineering: Oil and Gas Field Development Techniques: Editions TECHNIP.

Mavko, G., Mukerji, T., and Dvorkin, J. I., 2009, The Rock Physics Handbook: Cambridge University Press.

Stoffa, P. L., Jin, L., Sen, M. K., and Seif, R. K., 2008, Time-lapse seismic attribute analysis for a water-flooded reservoir: Journal of Geophysics and Engineering, **5**, 210 – 220.

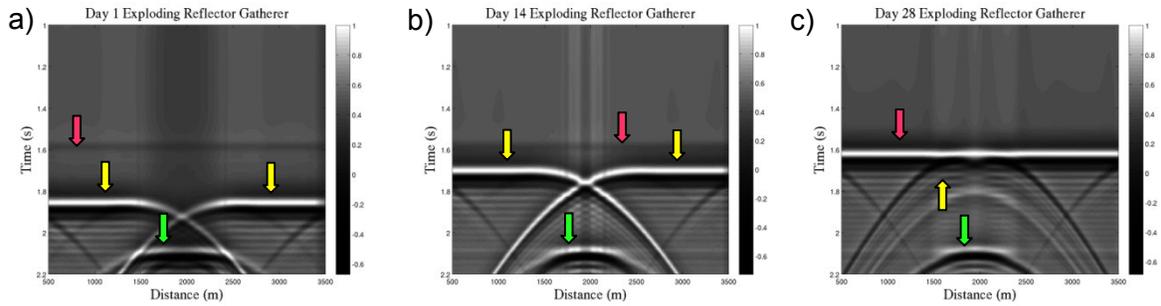Vracar, B. 2007, Pressure Transient Analysis, Tech. Rep, SAIT

Figure 1. 2D seismic models employing exploding reflector algorithm. Models show reservoir after day 1, 14 and 28. Stationary reservoir top and bottom are pointed to by red and green arrow, respectively. Non-stationary waterfronts, pointed to by yellow arrow.
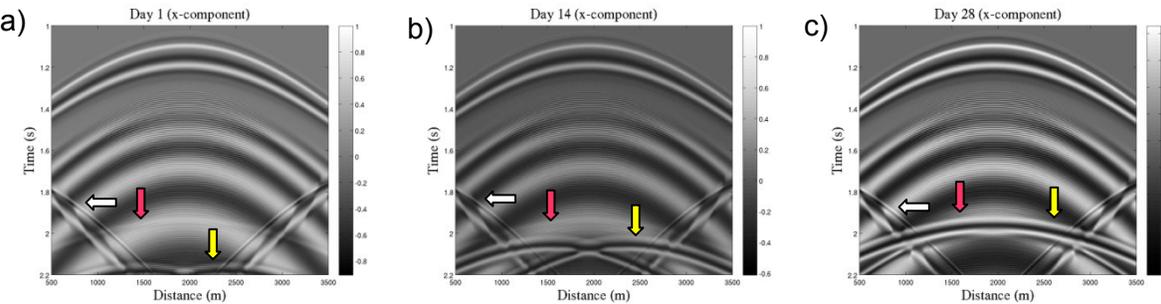

Figure 2. 3D seismic models employing shot gather algorithm, velocity x-component after day 1, 14 and 28. Models show S-waves. A projection of P-waves on to S-wave is seen as stationary reservoir top and non-stationary waterfronts, marked by red and yellow arrows. Boundary effects, marked by white arrow, show on reservoir sides.
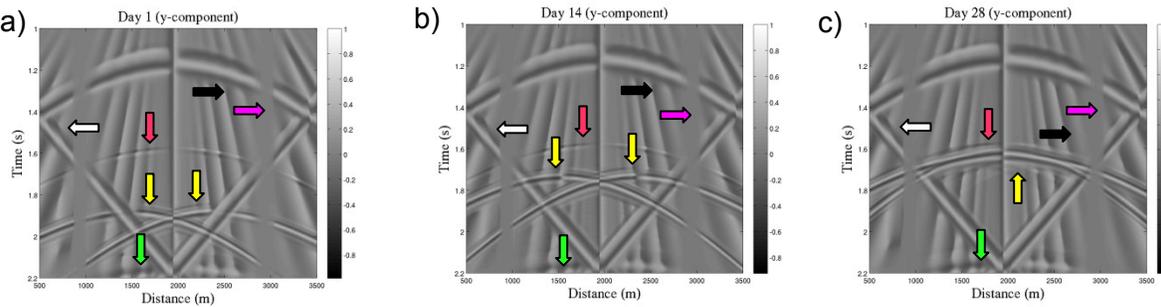

Figure 3. 3D seismic models employing shot gather algorithm, velocity y-component after day 1, 14 and 28. Models show converted waves. Stationary events such as reservoir top, bottom, boundary effects and numerical artifacts are pointed to by red, green, white and magenta arrow. Non-stationary events such as waterfronts are pointed to by yellow arrow. Rayleigh waves are pointed to by black arrow.
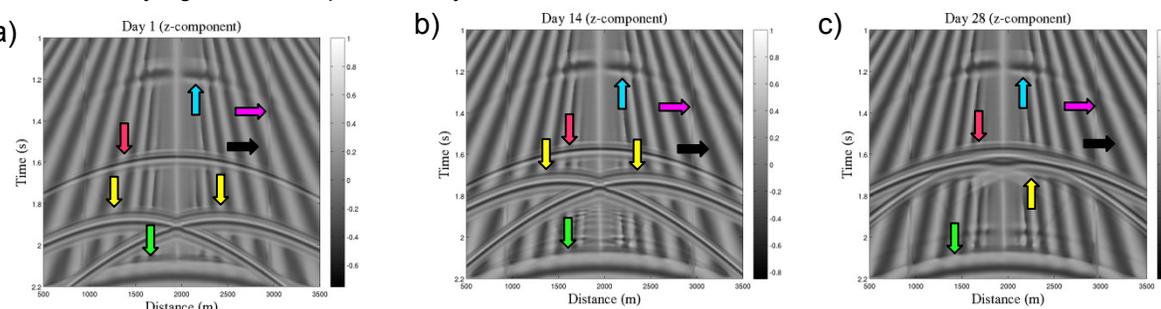

Figure 4. 3D Seismic Models employing shot gather algorithm, velocity z-component after day 1, 14 and 28. Models show P-waves. Stationary events such as reservoir top, bottom, S-wave projection onto P-wave and numerical artifacts are pointed to by red, green, turquoise and magenta arrow. Non-stationary events such as waterfronts are pointed to by yellow arrow. Rayleigh waves are pointed to by black arrow.